Journal of ELECTRONIC MATERIALS, Vol. 42, No. 5, 2013
DOI: 10.1007/s11664-013-2473-7
© 2013 TMS

Polarization-Engineered Enhancement-Mode High-Electron-Mobility Transistors Using Quaternary AlInGaN Barrier Layers

BENJAMIN REUTERS,[1,3,5] A. WILLE,[1,3] N. KETTENISS,[1,3] H. HAHN,[1,3] B. HOLLÄNDER,[2,3] M. HEUKEN,[1,4] H. KALISCH,[1,3] and A. VESCAN[1,3]

1.—RWTH Aachen University, GaN Device Technology, Sommerfeldstrasse 24, 52074 Aachen, Germany. 2.—Forschungszentrum Jülich GmbH, PGI9-IT, 52425 Jülich, Germany. 3.—Jülich Aachen Research Alliance, JARA-FIT, Jülich, Germany. 4.—AIXTRON SE, Kaiserstr. 98, 52134 Herzogenrath, Germany. 5.—e-mail: reuters@gan.rwth-aachen.de

Group III nitride heterostructures with low polarization difference recently moved into the focus of research for realization of enhancement-mode (e-mode) transistors. Quaternary AlInGaN layers as barriers in GaN-based high-electron-mobility transistors (HEMTs) offer the possibility to perform polarization engineering, which allows control of the threshold voltage over a wide range from negative to positive values by changing the composition and strain state of the barrier. Tensile-strained AlInGaN layers with high Al contents generate high two-dimensional electron gas (2DEG) densities, due to the large spontaneous polarization and the contributing piezoelectric polarization. To lower the 2DEG density for e-mode HEMT operation, the polarization difference between the barrier and the GaN buffer has to be reduced. Here, two different concepts are discussed. The first is to generate compressive strain with layers having high In contents in order to induce a positive piezoelectric polarization compensating the large negative spontaneous polarization. Another novel approach is a lattice-matched Ga-rich AlInGaN/GaN heterostructure with low spontaneous polarization and improved crystal quality as strain-related effects are eliminated. Both concepts for e-mode HEMTs are presented and compared in terms of electrical performance and structural properties.

Key words: AlInGaN, InAlGaN, composition, polarization, HEMT, enhancement mode

INTRODUCTION

Using quaternary AlInGaN barrier layers in GaN-based high-electron-mobility transistors (HEMTs) offers the possibility to realize depletion-mode (d-mode) and enhancement-mode (e-mode) operation.[1–3] By changing the composition and hence the spontaneous and piezoelectric polarization in a pseudomorphically grown AlInGaN layer, one can control the polarization difference between the AlInGaN barrier and the GaN buffer.[4,5] Tensile-strained AlInGaN layers with high Al contents and lattice-matched pure AlInN both generate high two-dimensional electron gas (2DEG) densities.[6,7] Compressively strained AlInN and AlInGaN layers have been used to generate a piezoelectric polarization which compensates a high spontaneous polarization to lower the 2DEG density and realize e-mode operation.[8,9] However, device performance is limited by the inferior crystal quality caused by the high In content. Further, barrier layers under high compressive strain show effects such as relaxation and In pulling, which degrade device characteristics even further and impede process control and reproducibility.[10,11] Here, we present a different approach of a simultaneously lattice-matched and polarization-reduced AlInGaN/GaN heterostructure

(Received August 9, 2012; accepted January 5, 2013; published online February 20, 2013)

with improved crystal quality showing performance competitive to other concepts for nitride-based e-mode transistors. A comparison with a compressively strained heterostructure is also given.

GROWTH CONDITIONS AND CHARACTERIZATION METHODS

In this work, we investigate HEMT structures grown on 2-inch sapphire substrates in an AIXTRON metalorganic vapor-phase epitaxy (MOVPE) reactor with standard precursors trimethylaluminum (TMAl), trimethylindium (TMIn), trimethylgallium (TMGa), ammonia (NH_3), and nitrogen (N_2) or hydrogen (H_2) as carrier gases. Growth was initiated with 10 s of Al preconditioning and an AlN nucleation layer with thickness of 6 nm deposited at 760°C, followed by 300 nm AlN and 2.5 μm GaN buffer layers, grown at 1250°C and 1070°C, respectively. Full spectroscopic *in situ* measurements of reflectance at different wavelengths between 276 nm and 775 nm by a measurement tool from LayTec with an additional true-temperature pyrometer module enables monitoring and control of the growth surface temperature and the growth rate during epitaxy.

Two series of samples with 8-nm- to 19-nm-thick AlInGaN barriers were grown, in which either the In content or the Al/Ga content ratio was changed dominantly. The composition adjustment was performed using the methodology presented in an earlier publication.[6] The In content in sample series 1 was controlled by using different growth surface temperature setpoints between 719°C and 825°C, and the Al/Ga content ratio in sample series 2 was varied by applying different TMAl-to-TMGa precursor ratios. A thin AlN interlayer between the GaN buffer and the quaternary barrier layer was grown under barrier reactor conditions at about 825°C in all heterostructures to enhance the carrier mobility in the HEMT structures.[7,12] The AlInGaN/GaN heterostructures of sample series 1 were capped with a thin (12 nm to 36 nm) GaN film for process-relevant issues, as reviewed elsewhere.[8]

Rutherford backscattering spectrometry (RBS) using 1.4-MeV He^+ ions at scattering angle of 170° was performed to acquire reliable information about the AlInGaN thickness and the exact depth-resolved composition. Details of the experimental setup were reported elsewhere.[13] Structural characterization of lattice constants, relaxation, and morphology was performed by high-resolution x-ray diffraction (HRXRD) and atomic force microscopy (AFM).

RESULTS AND DISCUSSION

One of the most important issues in AlInGaN/GaN heterostructures is accurate determination of the composition of the quaternary layers. Direct access to the composition for layers of small thickness below 20 nm is even more difficult. Measurements of the lattice constants by HRXRD are not a distinct method to determine the composition, because several compositions exhibit equal lattice constants. On the other hand, reliable RBS measurements can be performed on layers with a minimum thickness of about 30 nm. To overcome these limitations, several reference samples based on the layer structures of the HEMT samples with barrier thicknesses in the range of 48 nm to 75 nm were grown with reactor conditions identical to those used for the layers of the HEMT sample series. In Fig. 1, RBS spectra of two reference samples, grown at different surface temperatures, are exemplarily shown. It is clearly visible that the RBS signal for In is much larger for the reference sample grown at 719°C due to higher In incorporation at this temperature. By simulating the RBS spectra, a depth-resolved composition can be determined for these reference samples. The information about the composition at a specific depth can be used to simulate HRXRD 2Θ–ω (0002) scans of thinner layers to determine the composition most accurately.

The compositions of both HEMT sample series determined as described above are illustrated in Fig. 2 as a function of either the growth surface temperature or the TMAl-to-TMGa precursor ratio used in the experimental series. In series 1, In contents from 5% to 19% can be controlled by the growth surface temperature, as is obvious from the left image in Fig. 2. With lower surface temperature, it appears to be energetically favorable for the In incorporation to increase by mainly replacing Al atoms. In sample series 2, the Al/Ga content ratio is varied by using different TMAl-to-TMGa precursor ratios in the range between 0.17 and 2.38, which results in Al (Ga) contents from 11% (87%) to 54% (41%), as illustrated in the right image of Fig. 2. The In content is simultaneously increased from 2% to 5% for larger TMAl-to-TMGa precursor ratios, most likely due to a catalyst effect of TMAl for the

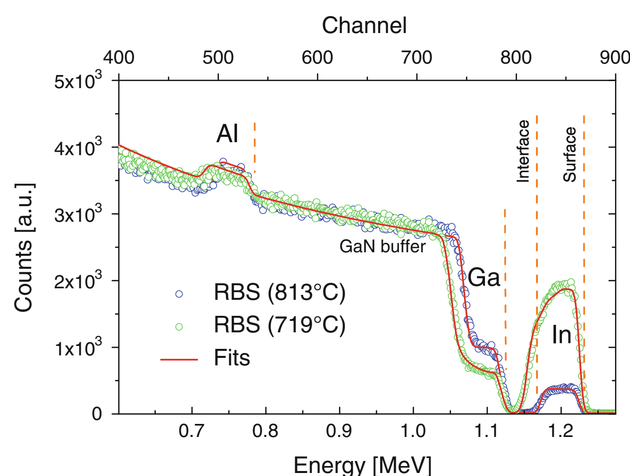

Fig. 1. RBS spectra of 70-nm- to 75-nm-thick reference samples grown at different surface temperatures of 813°C (blue dots) and 719°C (green dots), respectively. The red curves are simulations of (depth-resolved) compositions of the quaternary layer.

formation of In-rich phases, related to the low miscibility of InN and AlN.[14–16]

By changing the composition of the quaternary layers, the strain state also changes. The in-plane strain ε_{xx} in a pseudomorphically grown layer is calculated by Eq. (1) with nominal lattice constants calculated by Vegard's law, taking the composition from RBS into account.

$$\varepsilon_{xx} = \frac{a_{\mathrm{AlInGaN,strained}} - a_{\mathrm{AlInGaN,nom}}}{a_{\mathrm{AlInGaN,nom}}}. \quad (1)$$

In Fig. 3, the bandgap, calculated using a weighted formula from Ref. 1, is plotted as a function of the nominal lattice constant a, calculated by Vegard's law. Here, the bowing parameters are updated by the latest results from the literature: The bowing parameters used here are 0.9 eV for AlGaN,[17] 1.65 eV for InGaN,[17] and a quite high and constant value of 5.2 eV for AlInN.[11,18] The bowing parameter for AlInN is still vague and might also be In dependent, especially for the In-rich region.[17] The contour lines in the quaternary area illustrate the total polarization of quaternary barriers for the corresponding barrier composition, being pseudomorphically grown on a GaN buffer. The thicker red line indicates polarization matching to GaN. The total polarization P_{total} is the sum of the spontaneous P_{spon} and piezoelectric polarization P_{piezo}, taking formulas from the literature into account.[1–4]

The investigated sample series are also illustrated in Fig. 3. Both series start with high Al content of 51% and 62% (In content of 5%), which generates high tensile strain and results in a high polarization difference from GaN. The two sample series represent different approaches to lower the polarization difference. Sample series 1 shows an increasing In content from 5% to 19% for 16-nm-thick layers, which changes the strain state from high tensile strain ε_{xx} of 0.95% to high compressive strain, lowering the total polarization. Finally, sample A with thickness of 8 nm and In content of 17% (and high Al content of 48%) is under high compressive strain of –0.73%, which results in a low total polarization of $-3.99\ \mu\mathrm{C/cm^2}$. The In incorporation at the lowest surface temperature of 719°C is thickness dependent because of In pulling effects, which are observed for compressively strained layers.[11] This is also obvious in the RBS spectrum in Fig. 1 for the 75 nm reference layer, which shows an increasing In signal from the interface to the surface.

The impact of strain on the relaxation of the quaternary layers was investigated by HRXRD (10–15) reciprocal-space mappings (RSMs) shown in Fig. 4. For this analysis, two quaternary layers with different thicknesses of 8 nm and 16 nm at the growth conditions of sample A were used. The observation of the quaternary peak of the 8-nm-thick $Al_{48\%}In_{17\%}Ga_{35\%}N$ layer, shown in the left image of Fig. 4, is

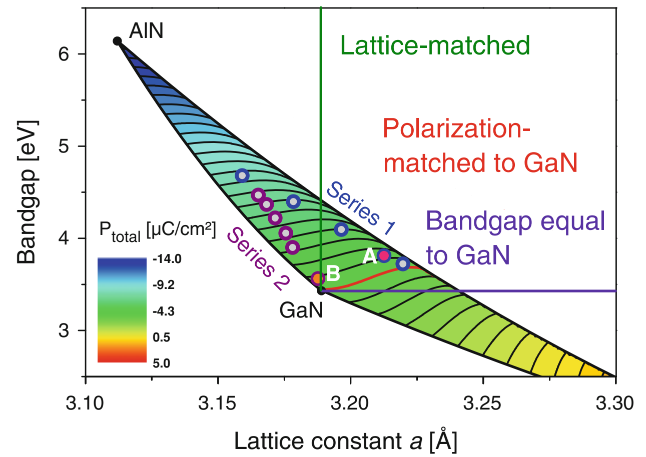

Fig. 3. Calculated AlInGaN bandgaps, employing the compositions determined by RBS, plotted over the lattice constant a. The lattice constants are calculated by Vegard's law. Samples A and B, which are finally processed as field-effect transistors, are marked in pink and orange color, respectively.

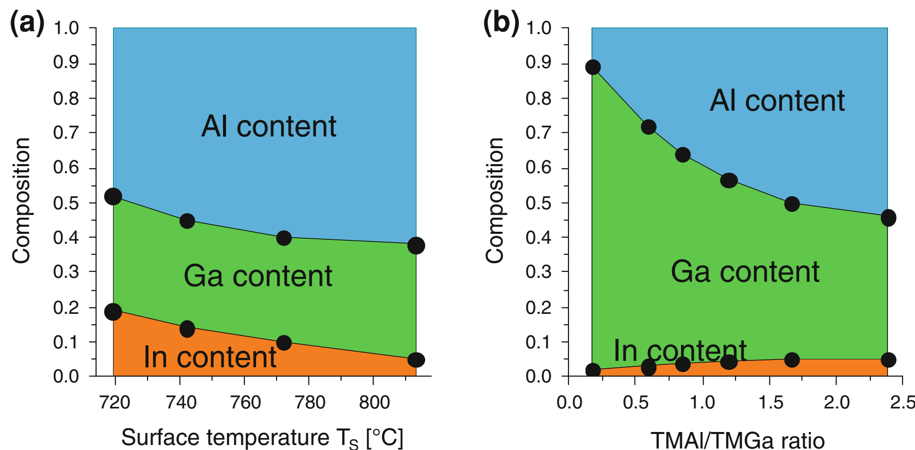

Fig. 2. Area plots of the composition of the quaternary AlInGaN layer: (a) increasing In content with lowered surface temperature for sample series 1, and (b) increasing Al content with higher molar flow TMAl/TMGa ratios for sample series 2.

difficult, because the peak partly overlaps with the GaN buffer peak and the intensity of this very thin layer is low. Nevertheless, there is no indication for relaxation of this layer, because all counts are detected at a Q_x value equal to that of the GaN peak. A completely different peak shape emerges for the 16-nm-thick layer with a slightly higher In content of 19%, which shows a clear, broadened peak shifted to lower Q_x values and larger Q_z values. This is a clear indication for relaxation and proves that the critical thickness at compressive strain of -0.73% lies in the range between 8 nm and 16 nm.

Sample series 2 starts from tensile strain ε_{xx} of 0.75% and moves to the lattice-matched line by reducing the Al-to-Ga content ratio, as illustrated in Fig. 3. Sample B almost matches the lattice constant of GaN (ε_{xx} = 0.04%) and exhibits low total polarization of -3.79 μC/cm^2. The changing composition of sample series 2, exemplarily, is manifested in the HRXRD 2Θ–ω (0002) scans shown in Fig. 5, which show the AlInGaN peak shifting to lower diffraction angles for reduced Al contents. HRXRD (10–15) RSMs reveal pseudomorphic growth for all layers of sample series 2. The simulations of the HRXRD 2Θ–ω scans are consistent with the RBS compositional analysis. Fringe oscillations reveal the thicknesses and hence the growth rates of the quaternary layers. They increase from 4.7 nm/min to 6.3 nm/min for lower Al and larger Ga contents and can be explained by a higher growth rate of GaN in comparison with AlN.

Both samples A and B, which were finally processed, show similar, low total polarization of -3.99 μC/cm^2 and -3.79 μC/cm^2, respectively, near to the spontaneous polarization of GaN of -3.39 μC/cm^2.[4] This is also obvious in Fig. 3, because both layers are located on almost the same polarization contour line. While sample A generates positive piezoelectric polarization by inducing high compressive strain, which compensates the spontaneous polarization, sample B simply has low spontaneous polarization with negligible piezoelectric polarization, because it is nearly lattice-matched.

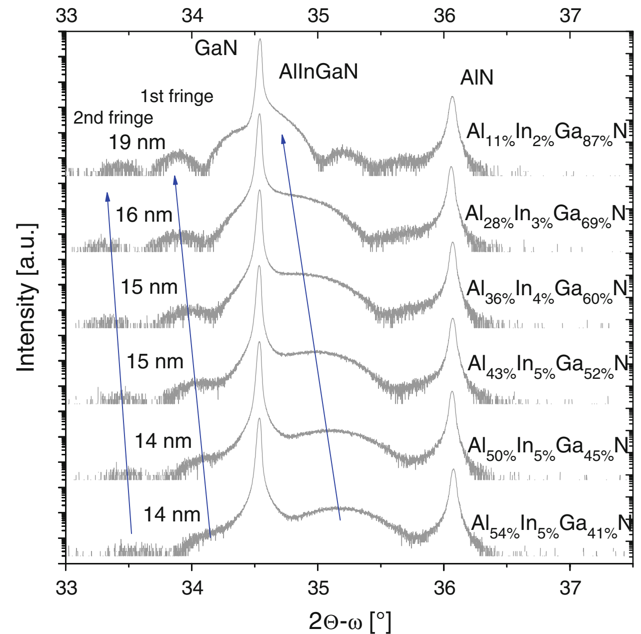

Fig. 5. HRXRD (0002) 2Θ–ω scans for sample series 2 with varying Al/Ga content ratio. The blue lines in the figure are guides to the eye to indicate the quaternary peak position and the first and second fringe position.

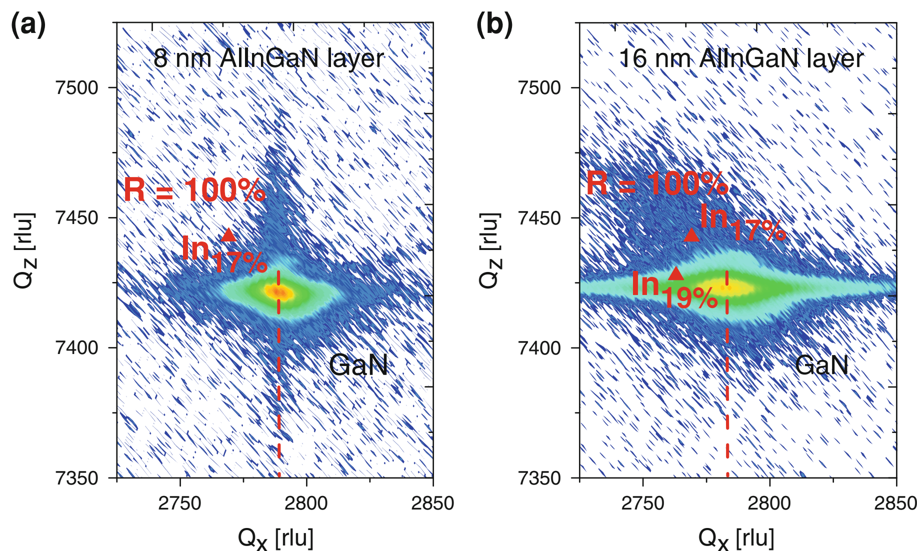

Fig. 4. HRXRD (10–15) reciprocal-space mappings (RSMs) of AlInGaN samples grown at equal reactor conditions with thickness of 8 nm (a) and 16 nm (b), Al content of 48%, and In content of 17% to 19%. The patterned red line illustrates pseudomorphic growth, as observed for the 8 nm layer (a). The red triangles show the theoretical position of fully relaxed layers with the given In content. The 16 nm layer (b) shows relaxation, which is manifested by a broadened AlInGaN peak shifted to lower Q_x values and larger Q_z values.

Hall and van der Pauw measurements were carried out on nonprocessed epiwafers to determine the 2DEG density and the carrier mobility. The mobility as a function of 2DEG density of both sample series is plotted in Fig. 6. Additionally, the dotted lines (orange) represent equal sheet resistance contours. Both series start from values near the 200 Ω/sq line, which is typical for high-polarization AlInN/GaN heterostructures for d-mode application. By reducing the 2DEG density, it is possible to increase the sheet resistance to above 10 kΩ/sq, which is promising for achieving e-mode operation.

While sample series 1 reduces the 2DEG density by incorporating more In, due to a lower growth surface temperature, sample series 2 lowers the Al content by changing the precursor flow. These different approaches have a dramatic influence on the carrier mobility. A strong decrease is observed for series 1, most likely caused by lower crystal quality, which is manifested by wider HRXRD RSM reflection peaks, due to relaxation (Fig. 4) and rougher interfaces for higher In contents.[6] The root-mean-square (rms) roughness on 5 μm × 5 μm for about 70-nm- to 75-nm-thick reference layers increases from values of 0.5 nm for 5% In to 1.5 nm for 29% In.

A different behavior is observed for sample series 2. The mobility is even increasing for lower 2DEG densities with a maximum of 1820 cm^2/Vs at 300 K and 10,900 cm^2/Vs at 77 K for a 2DEG density of about 7×10^{12} cm^{-2}. These values are among the highest ever reported for In-containing barrier layers and similar to values of AlGaN HEMTs, which might be a hint that tuning the 2DEG densities and mobilities between AlGaN and AlInN is possible with the quaternary material system.[19] The high mobility values are consistent with the low surface roughness of all layers of sample series 2 in the range of 0.4 nm to 0.6 nm.

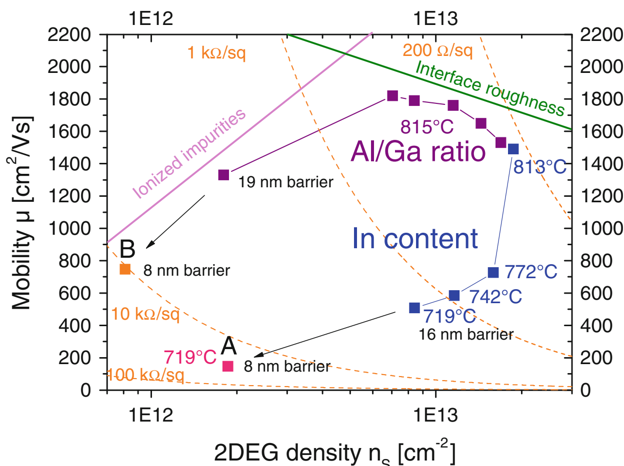

Fig. 6. 2DEG mobility as a function of 2DEG carrier density by Hall and van der Pauw measurements. Lines for dominant scattering mechanisms are shown as a guide to the eye. The dotted lines are hyperboles of equal sheet resistance.

Reducing the 2DEG density further leads to a drop of the mobility, which results in a peak-like shape of the mobility against the 2DEG density. While the mobility of sample series 1 is limited by increasing roughness correlated to the higher In content, the dominant scattering mechanisms for sample series 2 are different: the width and position of the 2DEG changes with varying 2DEG densities, which results in different dominant scattering mechanisms.[20] For densities above 7×10^{12} cm^{-2}, the distance of the 2DEG from the interface becomes small, therefore interface scattering becomes the dominant mechanism here. For the samples of series 2, all of which have similar interface roughness, we observe exactly the aforementioned behavior. This leads to the conclusion that the reduction of the mobility at high 2DEG densities is caused by a lower distance from the interface. For lower densities below 7×10^{12} cm^{-2}, carrier confinement becomes worse and carriers propagate into the GaN buffer. Here, ionized impurities are the major cause for enhanced scattering and the resulting lower mobility. These results show that the mobility is strongly dependent on the accumulated sheet carrier density in the 2DEG and the corresponding carrier confinement. The interface roughness is only a limiting factor in the region of higher 2DEG density. Consequently, designs with low on-resistance could be envisioned, in which a combination of low- and high-polarization layers could be used to reduce the access resistance and simultaneously sustain the e-mode character of the active region.[21]

Both samples A and B with 8-nm-thick quaternary barriers, also shown in Fig. 6, exhibit very low 2DEG densities of 1.8×10^{12} cm^{-2} and 0.8×10^{12} cm^{-2}, respectively, due to the previously discussed low total polarization in these layers. These samples were finally processed to field-effect transistors with 1 μm gate length. Details on the processing and the different device concepts are published elsewhere.[8,19] The different device geometries make direct comparison quite difficult. The varying distance of the gate contact from the 2DEG is the most relevant difference in the device design. While for the lattice-matched sample B the gate-to-2DEG distance is the barrier thickness of 8 nm only, for the compressively strained sample A it is about 30 nm, consisting of the 8 nm barrier, 12 nm GaN cap, and 10 nm dielectric. However, bearing this difference in gate-to-source capacitance in mind, the observed trends in device performance can also be very well correlated to structural properties. Here, the discussion is restricted to some distinctive electrical parameters, derived from the transfer characteristics of samples A and B, shown in Fig. 7. For comparison, values of electrical and structural properties are presented in Table I.

Clearly visible in the transfer characteristics, shown in Fig. 7, is the e-mode behavior of both samples A and B with threshold voltage of V_{th} of 0.56 V and 0.20 V, respectively. The nearly

lattice-matched sample B shows superior performance. The drain current (at 3 V) is 338 mA/mm, which is three times higher than that of sample A (96 mA/mm), and the extrinsic (intrinsic) transconductance is improved by a factor of four (six) to 165 mS/mm (370 mS/mm) for the lattice-matched sample B. The better performance must be attributed to several effects. Theoretical calculations of the intrinsic transconductances of both devices, presented in Table I, show that the difference in gate-to-source capacitance by a factor of about four plays a major role here, but cannot fully explain the sixfold larger intrinsic transconductance. Hence, the lower sheet resistance in the access region of 1.4 kΩ for sample B in comparison with 2.2 kΩ for sample A and the improved 2DEG mobility under the gate from 146 cm^2/Vs to 747 cm^2/Vs at 300 K contribute strongly to the better performance. The better mobility can be attributed to a supposable decreased interface roughness for lower In contents, which is evidenced by the improved morphology in AFM scan.

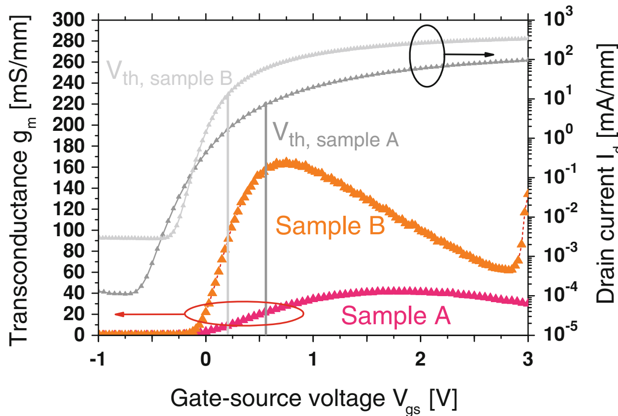

Fig. 7. Transfer characteristics of AlInGaN/GaN heterostructures (samples A and B) with low polarization difference showing enhancement-mode behavior. The drain–source voltage V_{ds} is 10 V.

The two devices behave differently in the subthreshold regime. The drain current of sample A shows a less steep slope than sample B, probably caused by additional interface traps due to the GaN cap and the gate dielectric.[22] Another effect of the additional dielectric and the higher gate-to-channel distance is a reduction of the leakage current in off-state at −1 V from 3×10^{-3} mA/mm for sample B to 1×10^{-4} mA/mm for sample A. As a result, the drain current I_{on}/I_{off} ratio is increased by one order of magnitude to 10^7 for sample A. Furthermore, sample B shows a four orders of magnitude higher gate leakage current in forward direction, exceeding 1 mA/mm at 1.15 V, due to the missing dielectric. Further details on the electrical performance of these devices can be found elsewhere.[8,21]

The theoretically smaller conduction-band offset for sample B, due to the lower bandgap of 3.56 eV in comparison with 3.81 eV for sample A, might negatively impact electron confinement in the 2DEG, which could lead to higher leakage currents. On the other hand, nanoscale phase separation is stronger in quaternary layers with higher In contents.[15] This results in In clustering and hence spatial fluctuations in the band structure.[16] The effective bandgaps might not differ as strongly as calculated above for both samples. At this point, based on just two samples with differences in barrier composition and device geometry, more precise analysis of the separate effects of composition, bandgap, and dielectric on leakage current is not possible. However, from the presented experiments, it seems favorable to use a gate dielectric in order to suppress leakage currents in In-containing hetero field effect transistor (HFET) structures.

CONCLUSIONS

Two different approaches have been presented and realized to achieve e-mode operation by polarization engineering. The first approach uses high compressive strain to generate piezoelectric polarization for compensation of spontaneous polarization. Here, a high In content is necessary, which

Table I. Electrical and structural properties of the low-polarization samples A and B

Sample Composition	A $Al_{0.48}In_{0.17}Ga_{0.35}N$	B $Al_{0.11}In_{0.02}Ga_{0.87}N$
E_{gap} (eV)	3.81	3.56
P_{total} ($\mu C/cm^2$)	−3.99	−3.79
P_{spon} ($\mu C/cm^2$)	−5.07	−3.75
P_{piezo} ($\mu C/cm^2$)	1.08	−0.04
V_{th} (V)	0.56	0.20
$g_{m, max; ext. (int.)}$ (mS/mm)	42 (64)	165 (370)
$I_{d, 3V}$ (mA/mm)	96	338
R_{sheet} (access) (Ω/sq)	2.2 k	1.4 k
ε_{xx} (%)	−0.80	−0.04
μ (cm^2/Vs)	146	747
Roughness (nm)	1.5	0.6

results in inferior crystal quality and 2DEG mobility. Another disadvantage of this approach is the high compressive strain, which is critical for process control and reproducibility, because relaxation and In pulling occur. A much better approach is a non-strained nearly lattice-matched heterostructure with lower In contents and low Al content, so that the spontaneous polarization remains low. Both concepts allow realization of field-effect transistors showing e-mode behavior.

The epitaxial growth parameters that effectively modify the composition from high-Al-content layers under tensile strain to lattice-matched and compressively strained layers were discussed. Quaternary samples grown at relatively high temperatures of 825°C show mobilities of 1820 cm^2/Vs at 300 K and 10,900 cm^2/Vs at 77 K for a 2DEG density of about 7×10^{12} cm^{-2}. The mobility of polarization-reduced heterostructures shows strong sensitivity to the 2DEG density, which is applicable in device design. A simultaneously lattice-matched and polarization-reduced AlInGaN/GaN HFET was demonstrated and exhibited transconductance of 165 mS/mm. This emphasizes the great potential of that concept for e-mode devices.

ACKNOWLEDGEMENTS

This work was sponsored by the Deutsche Forschungsgemeinschaft (DFG).

REFERENCES

1. N. Ketteniss, L. Rahimzadeh Khoshroo, M. Eickelkamp, M. Heuken, H. Kalisch, R.H. Jansen, and A. Vescan, *Semicond. Sci. Technol.* 25, 075013 (2010).
2. N. Ketteniss, A. Askar, B. Reuters, A. Noculak, B. Holländer, H. Kalisch, and A. Vescan, *Semicond. Sci. Technol.* 27, 055012 (2012).
3. L. Rahimzadeh Khoshroo, N. Ketteniss, C. Mauder, H. Behmenburg, J.F. Woitok, I. Booker, J. Gruis, M. Heuken, A. Vescan, H. Kalisch, and R.H. Jansen, *Phys. Stat. Sol. C* 7, 2001 (2010).
4. O. Ambacher, J. Majewski, C. Miskys, A. Link, M. Hermann, M. Eickhoff, M. Stutzmann, F. Bernardini, V. Fiorentini, V. Tilak, B. Schaff, and L.F. Eastman, *J. Phys. Condens. Matter* 14, 3399 (2002).
5. V. Fiorentini, F. Bernardini, F. Della Sala, A. Di Carlo, and P. Lugli, *Phys. Rev. B* 60, 8849 (1999).
6. B. Reuters, A. Wille, B. Holländer, E. Sakalauskas, N. Ketteniss, C. Mauder, R. Goldhahn, M. Heuken, H. Kalisch, and A. Vescan, *J. Electron. Mater.* 41, 905 (2012).
7. M. Gonschorek, J.-F. Carlin, E. Feltin, M.A. Py, and N. Grandjean, *Appl. Phys. Lett.* 89, 062106 (2006).
8. H. Hahn, B. Reuters, A. Wille, N. Ketteniss, F. Benkhelifa, O. Ambacher, H. Kalisch, and A. Vescan, *Semicond. Sci. Technol.* 27, 055004 (2012).
9. S. Choi, H.J. Kim, Z. Lochner, Y. Zhang, and Y.-C. Lee, *Appl. Phys. Lett.* 96, 243506 (2010).
10. K. Lorenz, N. Franco, E. Alves, S. Pereira, I.M. Watson, R.W. Martin, and K.P. O'Donnell, *J. Cryst. Growth* 310, 4058 (2008).
11. B. Reuters, M. Finken, A. Wille, B. Holländer, M. Heuken, H. Kalisch, and A. Vescan, *J. Appl. Phys.* 112, 093524 (2012).
12. R. Butte, J.-F. Carlin, E. Feltin, M. Gonschorek, S. Nicolay, G. Christmann, D. Simeonov, A. Castiglia, J. Dorsaz, H.J. Buehlmann, S. Cristopoulos, G. Baldassarri Höger von Högersthal, A.J.D. Grundi, M. Mosca, C. Pinquier, M.A. Py, F. Demangeot, J. Frandon, P.G. Lagoudakis, J.J. Daumberg, and N. Grandjean, *J. Phys. D* 40, 6328 (2007).
13. B. Holländer, H. Heer, M. Wagener, H. Halling, and S. Mantl, *Nucl. Instrum. Methods Phys. Res. Sect. B* 161–163, 227 (2000).
14. M. Marques, L.K. Teles, L.M.R. Scolfaro, L.G. Ferreira, and J.R. Leite, *Phys. Rev. B* 70, 073202 (2004).
15. S. Nagarajan, T.S. Oh, M. Senthil Kumar, C.-H. Hong, and E.-K. Suh, *Jpn. J. Appl. Phys.* 47, 4413 (2008).
16. X.A. Cao and Y. Yang, *Appl. Phys. Lett.* 96, 151109 (2010).
17. E. Sakalauskas, B. Reuters, L. Rahimzadeh Khoshroo, H. Kalisch, M. Heuken, A. Vescan, M. Röppischer, C. Cobet, G. Gobsch, and R. Goldhahn, *J. Appl. Phys.* 110, 013102 (2011).
18. W. Terashima, S.-B. Che, Y. Ishitani, and A. Yoshikawa, *Jpn. J. Appl. Phys.* 45, L539 (2006).
19. N. Ketteniss, H. Behmenburg, L. Lecourt, N. Defrance, V. Hoel, J.C. De Jaeger, M. Heuken, H. Kalisch, and A. Vescan, *Semicond. Sci. Technol.* 27, 035009 (2012).
20. M.N. Gurusinghe, S.K. Davidsson, and T.G. Andersson, *Phys. Rev. B* 72, 045316 (2005).
21. N. Ketteniss, B. Reuters, B. Holländer, H. Hahn, H. Kalisch, and A. Vescan, *IEEE Device Research Conference Penn State*, 161 (2012).
22. R. Wang, P. Saunier, X. Xin, C. Lian, X. Gao, S. Guo, G. Snider, P. Fay, D. Jena, and H. Xing, *IEEE Electron. Device Lett.* 31, 1383 (2010).